Research in Astronomy and Astrophysics, 23:115020 (15pp), 2023 November https://doi.org/10.1088/1674-4527/acf442

Optical and X-Ray Studies of Marginal Contact Binary RW Dor Using TESS and XMM-Newton Observatories

K. Sriram and G. Mamatha Rani
Department of Astronomy, Osmania University 500007, India; astrosriram@yahoo.co.in
Received 2023 February 24; revised 2023 May 13; accepted 2023 May 30; published 2023 October 11

Abstract

Marginal short-period contact binaries are important to understand as they pose a different physical scenario than the predicted theoretical model based on the thermal relaxation oscillation mechanism due to their shallow degree of contact. Here we present the optical and X-ray studies of a contact binary source RW Dor using the Transiting Exoplanet Survey Satellite (TESS) and XMM-Newton telescopes. For the first time we report the varying O'Connell effect and explain the asymmetry with a spot model. Based on the new times of minima, we make a robust estimate of the orbital period of the third body at $47.01 \sim 0.52$ yr with an eccentricity $e = 0.21$. We show that the period-decreasing trend observed in $O - C$ variation can be explained by both conservative mass transfer from primary to secondary and AML via stellar wind. The X-ray luminosity exhibited by RW Dor did not vary significantly on three different occasions and was found to be about 3.34×10^{29} erg s^{-1}. Assuming that the quiescent X-ray emission is emitted from an undisturbed loop structure, the loop size is estimated to be 0.6–1 $\times 10^{10}$ cm which is $\leqslant$Alfvén radius $r_A \sim 8 \times 10^{10}$ cm.

Key words: (stars:) binaries (including multiple): close – X-rays: binaries – stars: activity

1. Introduction

Contact binaries are a subclass of close binary systems whose primary or secondary components have filled their Roche lobes and share a common convective envelope (CCE) with a varying degree of fill-out factor (Kopal 1959; Lucy 1968). The fundamental parameters of these binaries provide us with a better understanding of some of the most interesting physical processes, such as mass transfer, magnetic cycles, strong interactions between stars and stellar mergers (see Qian et al. 2017 for a detailed review). There exist two types of contact binaries, i.e., A- and W-subtypes based on the temperatures and masses (Binnendijk 1970). In the W-subtype, the primary eclipse is due to the more massive cooler component transiting the less-massive hotter component, and it is the opposite scenario for the A-subtype. Based on the long-term periodic studies, it also draws a picture of the presence of a third body in many such systems which can explain the low angular momentum configuration often observed in these systems. The optical imaging by Ruciński (1969) clearly indicates the presence of a third body in most contact binaries, explaining their pivotal dynamical role in the evolution of these systems. This was further confirmed by the $O - C$ diagram-based studies carried out on those binary systems.

Contact binaries are known to exhibit the O'Connell effect (O'Connell 1951) which is the asymmetry observed in the photometric light curve generally attributed to magnetic activity over the stellar surface. The synchronous fast rotation of common envelopes is somehow associated with the origin of X-ray emission (e.g., Gondoin 2004a). These systems exhibit high chromospheric activity along with high coronal emission and thus are strong X-ray emitters (Carroll et al. 1980; Huenemoerder et al. 2006; Hu et al. 2016). It has been observed that the strength of X-rays is correlated to the orbital period and also the temperature of binary companions (Stępien et al. 2001). It was noted that the massive component is responsible for the X-ray emission through their magnetic activity, e.g., VW Cep and YY Eri (Vilhu & Maceroni 2007). The Advanced Satellite for Cosmology and Astrophysics (ASCA) spectra displayed the characteristics of a corona and found two-component model temperatures of 7×10^6 K and 22×10^6 K along with a flux of 1×10^{-11} erg cm^{-2} s^{-1} and VW Cep appears to show polar spots based on Doppler imaging maps (Hendry & Mochnacki 2000). It has been found that magnetic loops in rapidly rotating low-mass stars would sweep to the poles (Buzasi 1997). Moreover, contact binaries display a super-saturation effect (McGale et al. 1996; Chen et al. 2006) and it has been argued that this effect is due to the large loops becoming unstable by the Coriolis force and being extended along the poles (Jardine & Unruh 1999). In this model, the loops are large and extended but Stępien et al. (2001) showed that the loops could be compact when compared to the stellar radius and spatially associated with the equatorial region of the stellar surface. The study of $O - C$ curves of overcontact binaries by Tran et al. (2013) using the Kepler satellite gave anticorrelated

$O-C$ curves for the primary and secondary eclipses that they interpreted as the outcome of the longitudinal movement of starspots on the stellar surface. A detailed study of $O-C$ curves indicates that the movement of a stellar spot is associated with the rotational motion of the individual star, and is asynchronous in 50% of the cases.

RW Doradus (RW Dor) is an interesting binary system with a short orbital period of 0.2854 day exhibiting G4/5 spectral type. The light curve displays a difference in the depth of minima and shows asymmetry in the light curve which was modeled as a hot spot in the massive component around the joining of the two stars (Marton et al. 1989). However, Kaluzny & Caillault (1989) did not find any significant asymmetry in the light curve, rejecting the idea of a spot over either of the stellar components. Marino et al. (2007) did observe asymmetry in the light curve but a strong O'Connell effect can be ruled out due to the large scatter in the maximum phase of the light curve. They also observed an orbital period that was decreasing with a rate of $\Delta P/P = -6.3 \times 10^{-11}$. In addition, Deb & Singh (2011) did not find any asymmetry in the light curve which was confirmed by the absence of a third light. Sarotsakulchai et al. (2019) did not find any observational signature of asymmetry in the light curve or O'Connell effect, strongly indicating no or a low level of stellar activity. They also found weak evidence of a decreasing period along with a cyclic trend in the $O-C$ curve, suggesting the possible presence of a third body. The radial velocity measurements found a spectroscopic mass ratio $q_{\rm sp} = 0.68$ with a similar spectral type exhibiting features of a K1 type star (Hilditch et al. 1992). Later, a similar $q_{\rm sp} = 0.63$ was reported by Duerbeck & Rucinski (2007) who found $V_o = 25\,{\rm km\,s^{-1}}$. Overall, these studies suggest that no strong activity has been observed in RW Dor with weak evidence of periodic variations in the respective light curve studies.

In the present work, we focus on the modeling of the light curve observed by the Transiting Exoplanet Survey Satellite (TESS) which displayed an O'Connell effect for the first time. Detailed studies have been performed to find a robust estimate of the periodic variation using previously published times of minima along with new ones with TESS and the All Sky Automated Survey (ASAS). We also studied the X-ray emission on different occasions observed by the XMM-Newton observatory to check the variations in the X-ray flux in the observed duration.

2. Observation and Data Analysis

TESS was placed at a stable orbit in a 2:1 resonance with the Moon following an elliptical orbit of 13.7 days (Ricker et al. 2015). The goal of the satellite is to look for exoplanets orbiting bright stars using the transit method. TESS observes the selected fields with a 10.5 cm optical telescope in the wavelength range of 600–1000 nm at 2100 pixel^{-1}. Its field of view is 2×96 deg^2 and scans the sky for 27 days. RW Dor was observed by TESS on two occasions, i.e., 2018 October 19 and 2018 December 15, with a cadence of 2 minutes. Pre-search Data Conditioning Simple Aperture Photometry (PDCSAP) data were used to study the light curve variation, and data were downloaded from the Mikulski Archive for Space Telescopes (MAST).[1]

We have also studied the archival data of the XMM-Newton observatory taken on three different occasions for the source RW Dor ($\alpha = 5^{\rm h}\ 18^{\rm m}\ 32\overset{\rm m}{.}5$, $\delta = -68^\circ\ 13'\ 32\overset{''}{.}7$) that was first observed on 2009 May 16 (ObsId.:0602980201) for 20.9 ks for which only data from the EPIC MOS1 camera were available. The second observation was on 2010 December 11 (ObsId.:0650020101) for a duration of 24.1 ks and was observed by both the EPIC MOS(1&2) and PN cameras. The third observation was on 2013 October 22 (Obs. ID:0723650201) for a duration of 20 ks and only EPIC MOS1&2 data were available. We have selected a circular source region and a background region having radius 50″ for our first and second observations, while for the third observation we have used a circular region with radius 35″ for both source and background regions. The source and background spectra were obtained using the expression "PATTERN < 12" for MOS data and "PATTERN < 4" for PN data using SAS version 19.1.0. We have obtained the redistribution matrix file and the ancillary response file utilizing rmfgen and arfgen tasks respectively. The spectral analysis was done employing XSPEC v 12.12.0 (Arnaud 1996).

3. TESS Detection of O'Connell Effect and Light Curve Solution

Previous optical studies of RW Dor have not reported any strong signature of stellar activity, i.e., O'Connell effect (for more details see Sarotsakulchai et al. 2019). The TESS PDCSAP light curve clearly exhibits the variable O'Connell effect (Figure 1, top panel). Figure 1 is obtained by taking the difference between the consecutive maxima in the observed light curve. During the first observation, which lasted for 25 days, a weak signature of O'Connell effect was observed, however, in the second span of observation, the effect was relatively evident. It can be seen that initially the O'Connell effect was not observed and gradually it started appearing. We fitted the phased light curve with and without the O'Connell effect (Figure 1, bottom panel). The light curve solutions were obtained using the Wilson–Devinney code-based program PHOEBE (Prsa & Zwitter 2005).

The following methodology was invoked to get the best solution for the light curves (for more details see Sriram et al. 2016, 2017, 2018). The primary component temperature was fixed at 5560 K based on a recent study by Sarotsakulchai et al. (2019) who constrained this value based on $B-V = 0.69$. We

[1] https://mast.stsci.edu

Table 1
Photometric Solutions Obtained for RW Dor Using TESS Data

	No Spot	With Spot
Parameter		
$A_1 = A_2$	0.50	0.50
$g_1 = g_2$	0.32	0.32
T_1(K)	5560	5560
T_2(K)	5200 ± 69	5200 ± 16
q	0.6147 ± 0.0063	0.6147 ± 0.0026
i^o	76.8334 ± 0.03	76.3580 ± 0.12
$\Omega_1 = \Omega_2$	3.0583 ± 0.0055	3.0816 ± 0.0034
r_1 (pole)	0.4042	0.4005
r_1 (side)	0.4294	0.4247
r_1 (back)	0.4626	0.4563
r_2(pole)	0.3195	0.3195
r_2 (side)	0.3343	0.3343
r_2 (back)	0.3672	0.36798
$L_1/(L_1+L_2)$	0.4459	0.4362
Spot colatitude (θ°)	⋯	32 ± 3
Spot longitude (ζ°)	⋯	40.3 ± 2.1
Spot radius ($r_{\rm spot}{}^\circ$)	⋯	15.2 ± 3.6
Temp. ratio	⋯	0.69 ± 0.08
$\Sigma w(o-c)^2$	0.0061	0.0052

fixed the gravity darkening coefficient $g_1 = g_2 = 0.32$ (Lucy 1967) and adopted albedos $A_1 = A_2 = 0.5$ for both components (Ruciński 1969). Bolometric limb darkening coefficients (logarithmic law) were adopted from the table determined by van Hamme (1993). A circular and synchronous ($F = 1$) orbit was assumed. Initially, four parameters were adjusted, i.e., the temperature of the secondary component (T_2), orbital inclination (i), the dimensionless potentials of the primary and secondary components ($\Omega_2 = \Omega_1$), and the luminosity of the primary star (L_1). The mass ratio was fixed at 0.63 based on the spectroscopic observations (Duerbeck & Rucinski 2007) and later freed along with other parameters to get the best solution. The best-fit solution resulted in a mass ratio $q = 0.614 \pm 0.006$ and an inclination $i = 77^\circ \pm 0.12$. The best-fit results are shown in Table 1 and the obtained values are similar to those reported in previous studies (Sarotsakulchai et al. 2019). In Figure 1, the middle panel displays the best fit using the black line. It is clear from the fit that a no-spot solution produces more residuals around phase 0.75. Later, we adopted a cool spot over the primary component and continued the fitting. The cool spot model has four parameters: the colatitude (θ), longitude (ξ), and radius of the spot ($r_{\rm spot}$) and spot temperature ratio ($T_{\rm spot}/T_{\rm star}$). The best-fit parameters are given in Table 1 after including a cool spot and finding the size of the stellar spot to be 15° at a colatitude of ∼32° during the Heliocentric Julian Date (HJD) 2458489.2509 to HJD 2458489.3079 and the temperature ratio is ∼0.65. In order to produce a robust the solution, we varied the primary component's temperature from 5400 to 5800 K and performed the fitting. The lowest residuals were noted to be the best solution which is displayed in Table 1 (Figure 1, bottom panel).

4. Period Variation Studies

Previous studies by Sarotsakulchai et al. (2019) observed a period-decreasing trend along with weak evidence of sinusoidal variation, indicating the possible presence of a third body with an orbital period of ∼50 yr. Many times of minima were older than 1940 and hence we used TESS data to make the study of the $O-C$ variation more robust. The new times of minima along with others are logged in Table 2. The TESS time units are converted to HJD using the utility mentioned in the link https://astroutils.astronomy.osu.edu/time/index.html. In order to completely determine the various parameters of the third body assuming cyclic variation, we applied Zasche's code (Zasche et al. 2009) in MATLAB which implements the Simplex method in order to arrive at best-fit solutions. The following equation was fitted to the overall $O-C$ diagram in Figure 2 using a red line and a blue line displays only the period-decreasing quadratic term.

$$\mathrm{Min.I} = \mathrm{JD}_o + \mathrm{P.E} + \mathrm{Q.E}^2 + \frac{a_{12}\sin i}{c} \times \left[\frac{1-{e_3}^2}{1+e_3\cos\nu}\sin(\nu+\omega_3) + e_3\sin(\omega_3)\right], \quad (1)$$

where $a_{12}\sin i$, c, e_3, ν and ω_3 are the projected semimajor axis, speed of light, eccentricity, true anomaly of the binary orbit around the center of mass of the triple system and the longitude of the periastron, respectively. Table 3 displays the best-fit values for various parameters for different times of minima in the initial three columns.

To make the analysis of the third body more robust, we varied the eccentricity of the third body, i.e., $e_3 = 0$–1 and allowed other parameters to vary, and noted the lowest residual at $e_3 = 0.21$. Later, we kept $e_3 = 0.21$ which was freed subsequently and obtained the best solutions (see Table 3). To confirm the third body orbital period, we took different times of minima as shown in Figure 2 and we found that the orbital period varied from 46 to 54 yr. The best period $P_3 = 46.90 \pm 0.73$ was obtained for $\mathrm{JD}_o = 2458435.0148$ based on the sum of the residuals. We also performed a similar analysis by considering the times of minima observed after the year 1980. Figure 3 shows the best fit and we noted a period of $P_3 \sim 26.55 \pm 1.13$ yr (see Table 3 last column).

To make the result even more robust, we randomly selected epochs after the year 1985 (see Table 2) and estimated the third body orbital period. The distribution of the period is depicted in the histogram (Figure 4, top panel) and it is clear that the peak is observed around 47 yr. A Gaussian profile is fitted to this peak which is displayed with a dashed line in Figure 4 (top panel) and the best fit resulted in a mean period of P_3 $\mu = 47.01$ and $\sigma = 0.52$ yr. The higher periods were sparse and resulted due to

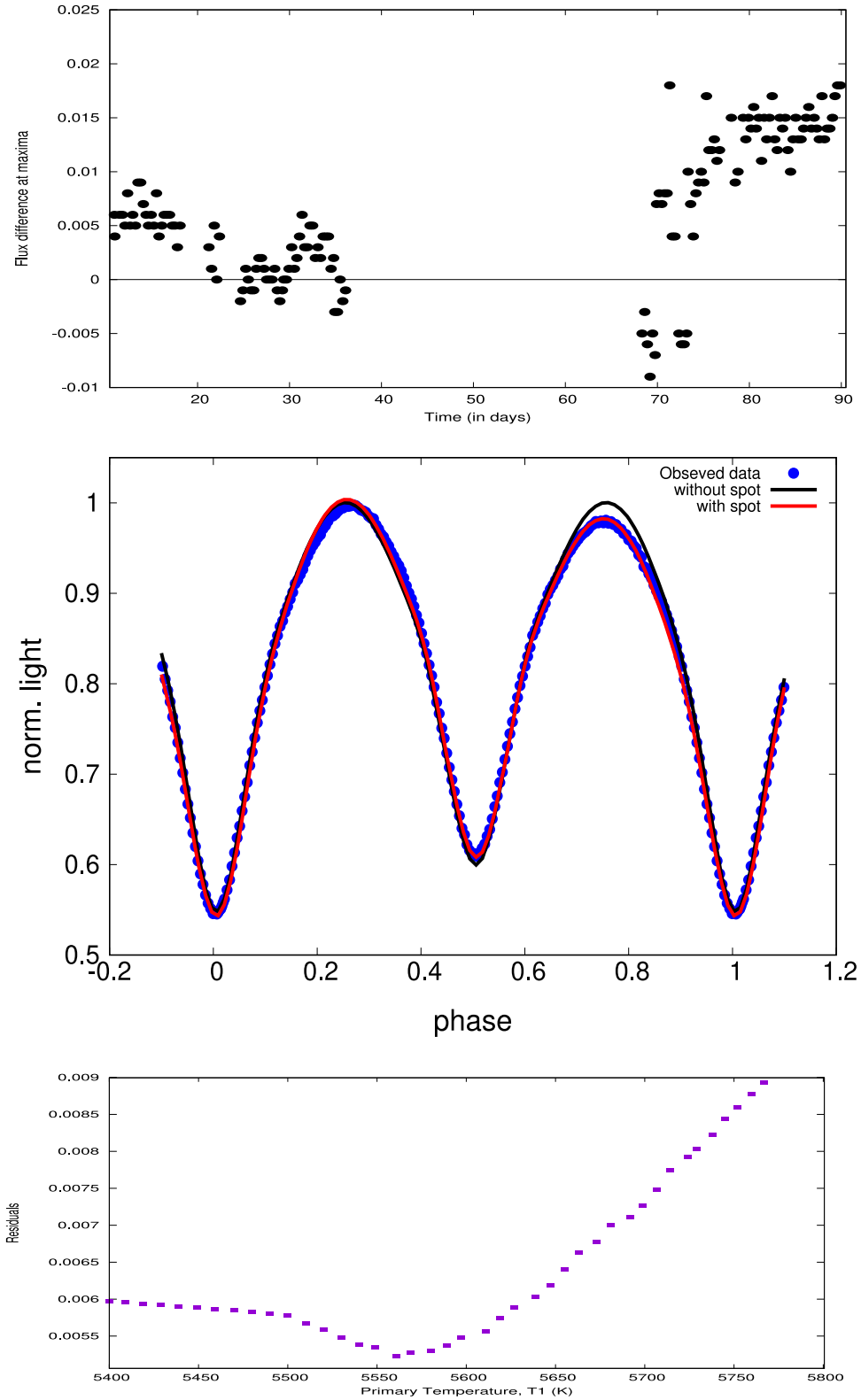

Figure 1. (a): Top panel displays the flux difference around the consecutive maximum and the dashed line at zero corresponds to the no O'Connell effect. It is clear that the O'Connell effect varies during the TESS observations. Time is in units of Barycentric Julian Date (BJD). (b): Middle panel displays fitted photometric solutions to the phased light curve along with a no spot solution (black line) and a spot solution (red line). (c): Bottom panel depicts the residual of the fits for different primary component temperature (T1) (see text for details).

Table 2
All Available Times of Minima for RW Dor

HJD(2400000)	Epoch	$(O-C)_1$	$(O-C)_2$	HJD(2400000)	Epoch	$(O-C)_1$	$(O-C)_2$	HJD(2400000)	Epoch	$(O-C)_1$	$(O-C)_2$
11298.835	−165122	−0.243777	0.0483927	14168.883	−155068	−0.240779	0.0125513	15621.901	−149978	−0.229449	0.00526872
16013.836	−148605	−0.235148	−0.00533002	16489.714	−146938	−0.223969	−3.09E-05	17075.903	−144884.5	−0.23324	−0.0164409
23784.6	−121383	−0.202202	−0.0589219	24172.537	−120024	−0.209419	−0.0699298	30938.602	−96322	−0.045714	0.0357531
44313.581	−49468.5	−0.007385	0.00443338	44464.876	−48938.5	−0.007774	0.00359874	44581.7728	−48529	−0.008073	0.00296067
44608.6063	−48435	−0.008095	0.00286148	44608.7488	−48434.5	−0.008326	0.00263007	44609.6063	−48431.5	−0.007215	0.00373861
44609.7493	−48431	−0.006947	0.0040062	44610.7487	−48427.5	−0.006668	0.00428233	44825.8462	−47674	−0.005538	0.00480244
44826.8442	−47670.5	−0.006658	0.00367964	44873.8038	−47506	−0.005722	0.00448457	44874.6594	−47503	−0.006511	0.00369319
44874.801	−47502.5	−0.007643	0.00256079	44958.5851	−47209	−0.006933	0.00303879	44961.5843	−47198.5	−0.005094	0.00486953
44961.7239	−47198	−0.008226	0.00173714	44962.5815	−47195	−0.007015	0.00294578	44962.7267	−47194.5	−0.004547	0.00541339
45021.6738	−46988	−0.005556	0.00424265	45049.5058	−46890.5	−0.006199	0.00352368	45049.6486	−46890	−0.00613	0.00359229
45050.6484	−46886.5	−0.005451	0.00426857	45076.4815	−46796	−0.006752	0.0028973	45370.6556	−45765.5	−0.002273	0.00659192
45370.6558	−45765.5	−0.002074	0.00679092	45370.6564	−45765.5	−0.001473	0.00739192	45376.6502	−45744.5	−0.002396	0.00645324
45376.6507	−45744.5	−0.001896	0.00695324	45376.6517	−45744.5	−0.000897	0.00795224	46680.7878	−41176	−0.002512	0.00321103
46681.7865	−41172.5	−0.002933	0.00278785	46690.7785	−41141	−0.003017	0.00268428	46695.7745	−41123.5	−0.00262	0.00307041
48500.047	−34803	0.000989	0.00330123	50559.9437	−27587	−0.003319	−0.0035325	50560.0865	−27586.5	−0.00325	−0.00346362
51158.5603	−25490	−0.00263	−0.00331136	51158.7027	−25489.5	−0.002962	−0.00364345	51505.682	−24274	−0.003938	−0.00483576
51505.8252	−24273.5	−0.00347	−0.00436784	51548.502	−24124	−0.003388	−0.00430966	51869.076	−23001	−0.004337	−0.00541813
54036.5947	−15408	−0.006196	−0.00745349	54036.7411	−15407.5	−0.002527	−0.00378445	54037.5995	−15404.5	−0.000516	−0.00177321
54037.7384	−15404	−0.004348	−0.00560517	54041.7335	−15390	−0.00573	−0.00698604	54049.5878	−15362.5	−0.001663	−0.00291681
54059.7177	−15327	−0.005699	−0.0069499	54087.9783	−15228	−0.005936	−0.0071786	54091.1189	−15217	−0.005429	−0.00667067
54095.115	−15203	−0.005811	−0.00705147	54107.6761	−15159	−0.005083	−0.00631966	55904.66718	−8864	−0.003588	−0.00373681
55906.8084	−8856.5	−0.003341	−0.00348787	56950.7446	−5199.5	−0.005332	−0.0043502	57112.6009	−4632.5	−0.006553	−0.00536357
57118.5968	−4611.5	−0.005376	−0.00417871	57446.7363	−3462	−0.005594	−0.00394823	57447.593	−3459	−0.005283	−0.00363601
57644.8485	−2768	−0.004716	−0.00278203	57645.8477	−2764.5	−0.004637	−0.00270154	57661.8334	−2708.5	−0.004865	−0.00290571
57686.6689	−2621.5	−0.004646	−0.00264951	57686.8119	−2621	−0.004377	−0.00238029	57720.639	−2502.5	−0.004643	−0.0025953
57721.6383	−2499	−0.004463	−0.00241379	57826.5461	−2131.5	−0.004316	−0.00210616	57827.5454	−2128	−0.004136	−0.00192461
TESS											
58411.0338	−84	−0.002108	0.00106413	58411.3185	−83	−0.002871	0.000301629	58411.6046	−82	−0.002234	0.000939127
58411.8898	−81	−0.002497	0.000676625	58412.1764	−80	−0.00136	0.00181412	58412.4608	−79	−0.002423	0.000751621
58412.7463	−78	−0.002386	0.000789119	58413.0319	−77	−0.002249	0.000926617	58413.3168	−76	−0.002812	0.000364116
58413.6028	−75	−0.002275	0.000901614	58413.8875	−74	−0.003038	0.000139112	58414.1738	−73	−0.002201	0.00097661
58414.4588	−72	−0.002664	0.000514108	58414.7444	−71	−0.002527	0.000651606	58415.0296	−70	−0.00279	0.000389105
58415.3157	−69	−0.002153	0.0010266	58415.6008	−68	−0.002516	0.000664101	58415.8867	−67	−0.002079	0.0011016
58416.1718	−66	−0.002442	0.000739098	58416.4576	−65	−0.002105	0.0010766	58416.7431	−64	−0.002068	0.00111409
58417.0281	−63	−0.002531	0.000651593	58417.3136	−62	−0.002494	0.000689092	58417.5994	−61	−0.002157	0.00102659
58417.885	−60	−0.00202	0.00116409	58418.17021	−59	−0.002273	0.000911587	58421.3102	−48	−0.002376	0.000814073
58421.5954	−47	−0.002639	0.000551572	58421.8809	−46	−0.002602	0.000589071	58422.1665	−45	−0.002465	0.00072657
58424.7358	−36	−0.002332	0.000864061	58425.0214	−35	−0.002195	0.00100156	58425.3068	−34	−0.002258	0.00093906
58425.5923	−33	−0.002221	0.000976559	58425.8775	−32	−0.002484	0.000714058	58426.163	−31	−0.002447	0.000751558
58426.7338	−29	−0.002573	0.000626556	58427.3045	−27	−0.002799	0.000401555	58427.5902	−26	−0.002562	0.000639055
58427.8757	−25	−0.002525	0.000676554	58428.1615	−24	−0.002188	0.00101405	58428.4467	−23	−0.002451	0.000751553
58428.7323	−22	−0.002314	0.000889053	58429.0178	−21	−0.002277	0.000926552	58429.3031	−20	−0.00244	0.000764052
58429.5889	−19	−0.002103	0.00110155	58429.8739	−18	−0.002566	0.000639051	58430.1593	−17	−0.002629	0.000576551
58430.4445	−16	−0.002892	0.000314051	58430.7303	−15	−0.002555	0.000651551	58431.0158	−14	−0.002518	0.00068905
58431.3015	−13	−0.002281	0.00092655	58431.5865	−12	−0.002744	0.00046405	58431.8721	−11	−0.002607	0.00060155
58432.1577	−10	−0.00247	0.00073905	58432.443	−9	−0.002633	0.00057655	58432.7283	−8	−0.002796	0.00041405
58433.0141	−7	−0.002459	0.00075155	58433.2996	−6	−0.002422	0.00078905	58433.5847	−5	−0.002785	0.00042655
58433.8702	−4	−0.002748	0.00046405	58434.1557	−3	−0.002711	0.00050155	58434.4415	−2	−0.002374	0.00083905
58434.7265	−1	−0.002837	0.00037655	58435.012	0	−0.0028	0.00041405	58435.2973	1	−0.002963	0.00025155
58435.583	2	−0.002726	0.00048905	58435.8683	3	−0.002889	0.000326551	58436.1573	4	0.000648	0.00386405
58436.4397	5	−0.002415	0.000801551								

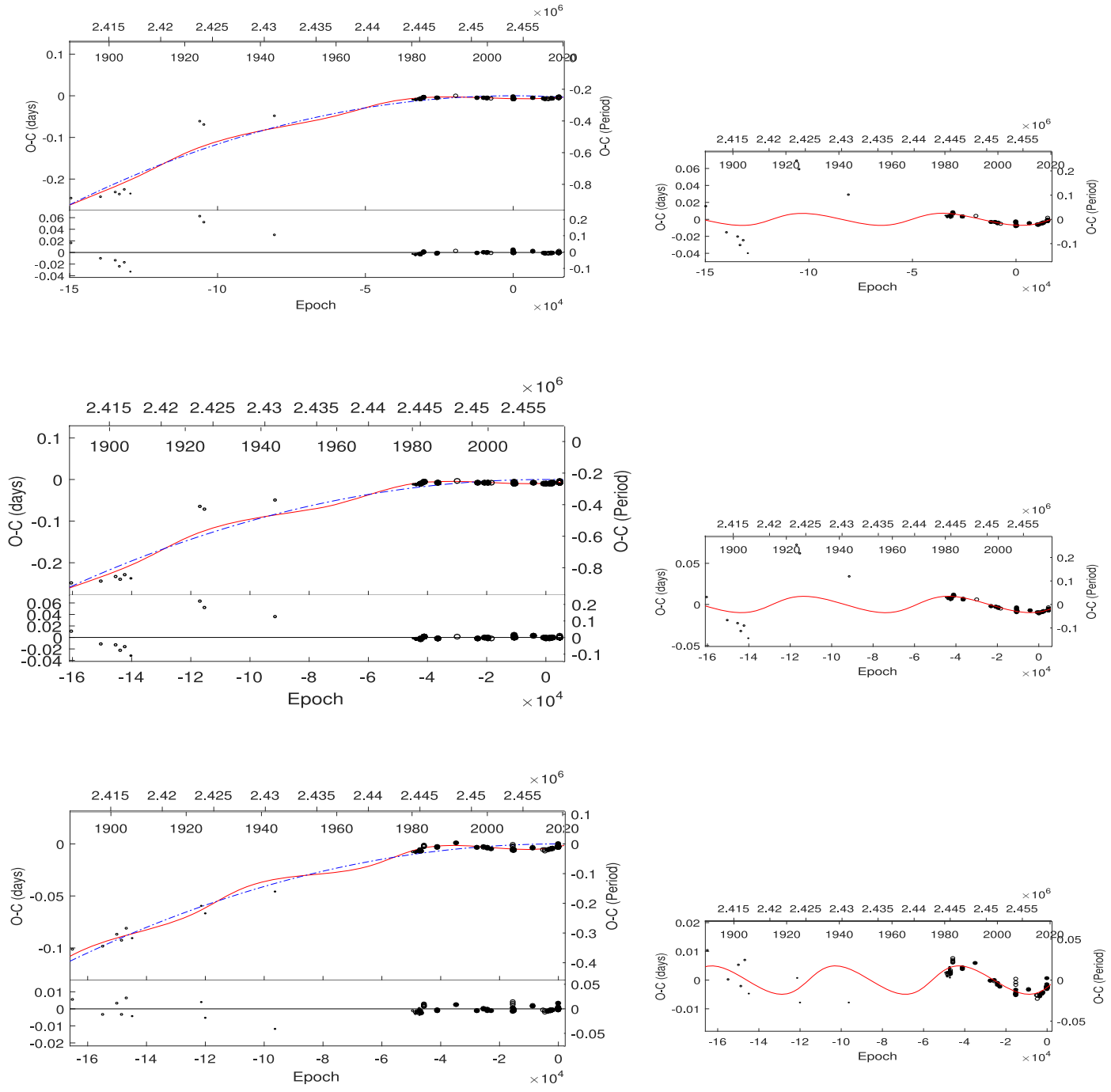

Figure 2. (a): The top panel displays the best-fit $O-C$ variations using LITE along with the residuals. The blue dashed line is a parabolic fit and the dashed line represents the LITE solution. (a′): The corresponding right panels show only the LITE fit to the data. Other panels display the same with different times of minima (see Table 2).

the older epochs. A very similar analysis was performed for the times of minima after the year 1980 which are relatively more robust. Figure 4 (bottom panel) displays the histogram along with a Gaussian fit with a dashed line. The best fit resulted in a mean period of P_3 $\mu = 27.22$ and $\sigma = 3.12$ yr.

5. X-Ray Spectral Analysis

We explored whether the X-ray emission of RW Dor varied during a span of four years as observed by the XMM-Newton telescope. It was done because previous studies did not observe any stellar activity in the form of the O'Connell effect

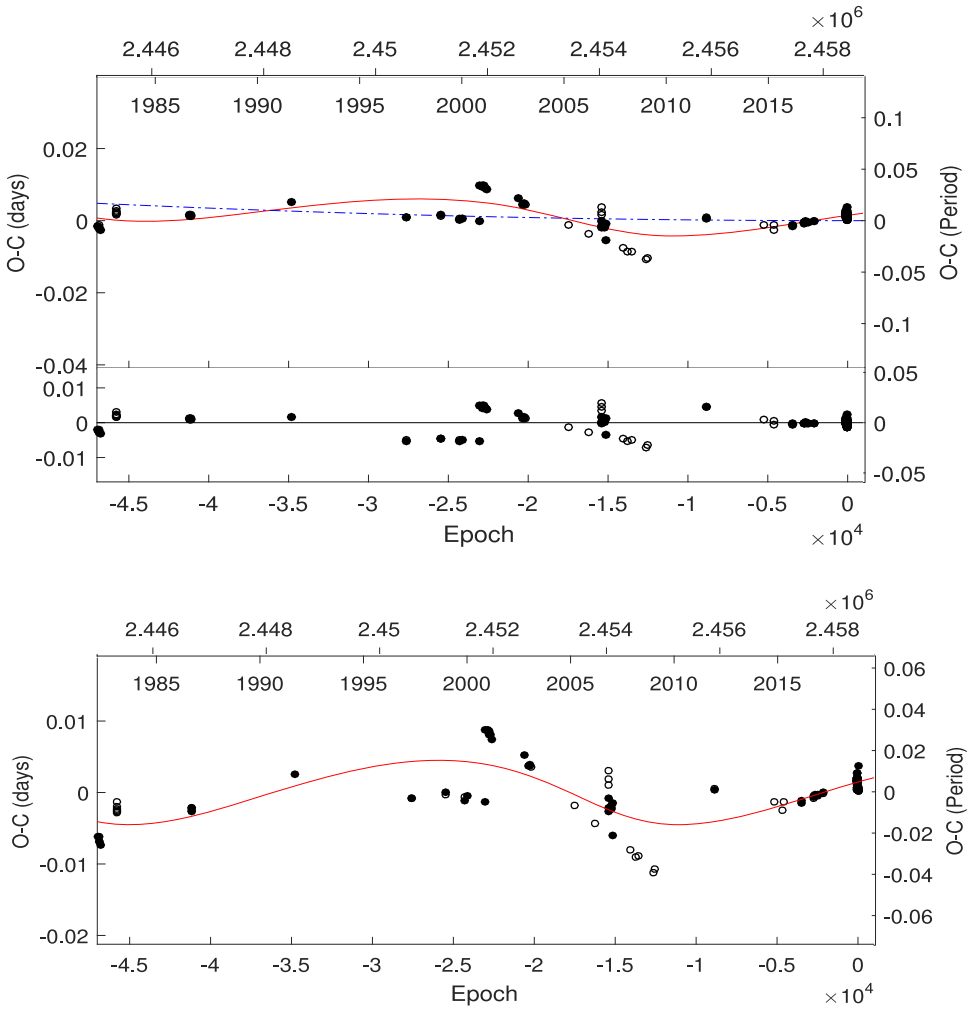

Figure 3. (a): Top panel: $O - C$ variations along with the LITE solution (red line) and quadratic fit (blue line). (b): The bottom panel displays the cyclic variation.

Table 3
Third-body Solution Based on $O - C$ Diagram for Different Epochs

Parameter	HJD = 2457112.6116	HJD = 2454037.5995	HJD = 2458435.0148	HJD = 2458436.4387
A, semi. amplitude (days)	0.0099 ± 0.0013	0.0045 ± 0.0018	0.0049 ± 0.0003	0.0045 ± 0.0004
P_3, period (yr)	54.51 ± 3.55	40.75 ± 2.88	46.90 ± 0.73	26.55 ± 1.13
e_3, eccentricity	0.21 ± 0.49	0.21 ± 0.71	0.21 ± 0.12	0.22 ± 0.16
ω_3, longitude of periastron passage	0.00 ± 78.11	9.183 ± 117.88	0.81 ± 22.42	211.60 ± 27.57
T_o, time of periastron passage	2440313.946 ± 5118.252	2443798.757 ± 4330.103	2442530.250 ± 1058.911	2454034.424 ± 735.439
a_{12} sin i, (au)	1.75 ± 0.23	0.801 ± 0.328	0.8751 ± 0.057	0.7953 ± 0.0740
Q	−0.0998 ± 0.00002	-0.0938 ± 0.00001	−0.111 ± 0.0001	−0.218 ± 0.0005
$f(M_3)$, $(M_\odot)$	0.0018 ± 0.000016	0.000311 ± 0.000001	0.00030 ± 0.000001	0.00071 ± 0.0000040
$M_3(M_\odot)_{i=90°}$	0.160 ± 0.00051	0.085 ± 0.00014	0.0852 ± 0.002	0.1147 ± 0.0002
$M_3(M_\odot)_{i=60°}$	0.187 ± 0.00060	0.099 ± 0.00017	0.100 ± 0.001	0.1336 ± 0.0003
M_3 $(M_\odot)_{i=30°}$	0.346 ± 0.0011	0.179 ± 0.00032	0.177 ± 0.002	0.2427 ± 0.0005
Sum of the square residuals	0.0116	0.0135	0.0016	0.0075

Note. The last column is obtained only for times of minima after the year 1985 (see text).

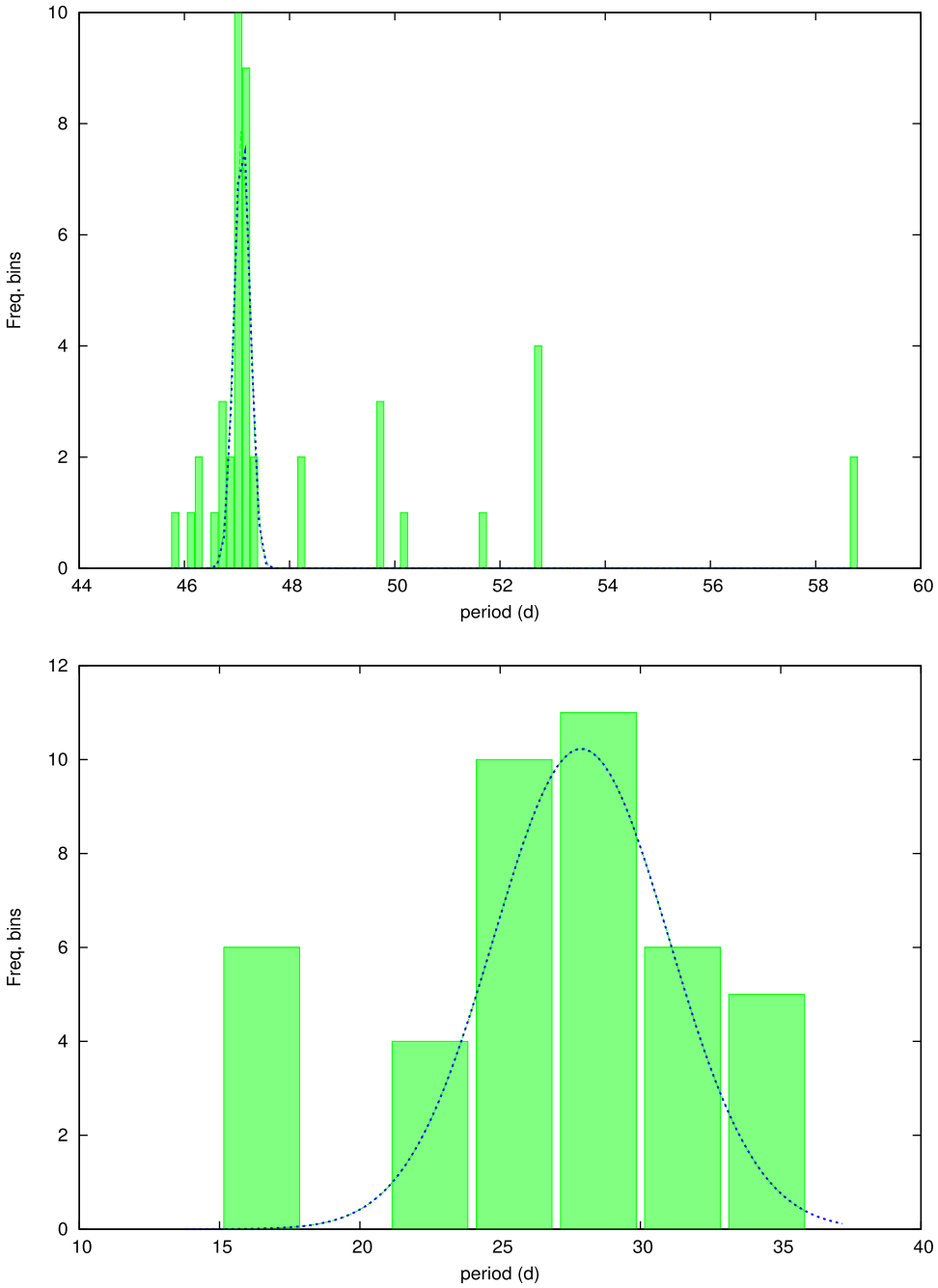

Figure 4. (a): Top panel: Histogram of the third body period obtained from the LITE solution with different epochs after the year 1985. The dashed line is a best-fit Gaussian profile with $\mu = 47.01$ and $\sigma = 0.52$. (b): Bottom panel: Same as above but with the LITE solution considering the data after 1985. The dashed line is a best-fit Gaussian profile with $\mu = 27.22$ and $\sigma = 3.12$.

(Sarotsakulchai et al. 2019). We fitted the X-ray spectra of MOS1, MOS2 and PN as shown in Figures 5–7. First, we tried with a simple power-law model to fit the spectra but the observed χ^2 were noted to be $\geqslant$2. Then we unfolded the spectra with wabs*bremsstrahlung and wabs*bbody models. The hydrogen column density was fixed to $5 \times 10^{20}\,\mathrm{cm}^{-2}$ based on Dicky & Lockman H I in the Galaxy (Dickey & Lockman 1990). In the case of the bremsstrahlung model, it was found that electron temperature was around $kT_e = 0.60\,\mathrm{keV}$ with a poor fit (Table 5). The blackbody

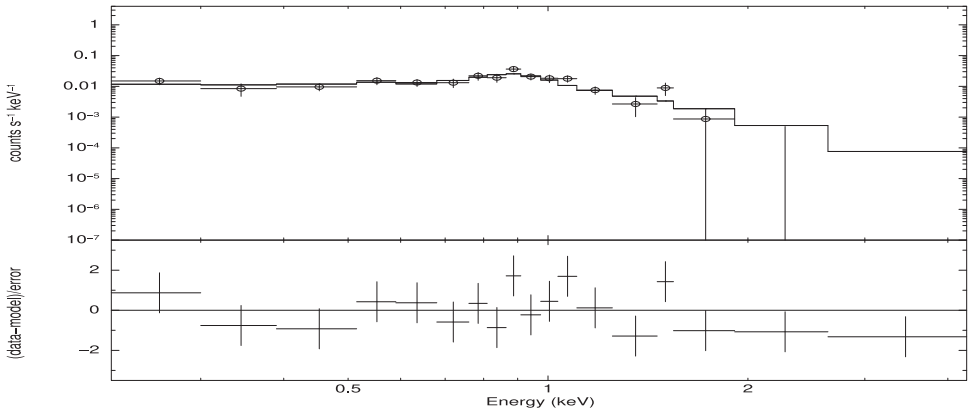

Figure 5. The top panel shows the unfolded spectrum along with the fit (thick line) for EPIC MOS1. The bottom panel displays the residuals. The reference number is ObsID.0602980201 and observation date is 2009 May 16.

temperature was about $kT \sim 0.17 \pm 0.02$ on all the occasions (Table 6), not displaying any variation.

Later we attempted a plasma model, i.e., apec model (Smith et al. 2001), which has two main parameters, viz. plasma temperature kT_e and abundance Z ($Z_\odot$). Initially, a single apec model resulted in a high χ^2, and hence a two-component apec model was used. The results are shown in Table 7 for Mos 1 and 2 and PN for different years. The $kT_1 = 0.24 \pm 0.08$ keV and $kT_2 = 0.93 \pm 0.15$ keV for the year 2010 along with flux 1.61×10^{-13} erg cm^{-2} s^{-1}. In general, if the source would have been active then the active coronal X-ray emission would have three or four components which was not evident from the present studies. The observed coronal temperatures strongly indicate the presence of a quiescent corona in RW Dor and found no significant variation from 2009 to 2013. The X-ray luminosity was estimated based on the distance determined from the Gaia parallax, i.e., $d = 123.57$ pc (Table 7).

6. Results and Discussion

6.1. Conservative Mass Transfer

For the first time, we report clear evidence of the variable O'Connell effect in RW Dor. Based on the photometric solutions, we observed that a cool spot of size 15° at a latitude of 60° on the primary component is necessary for the best fit. The photometric solution mass ratio was found to be $q = 0.61$ with an inclination of 77° which is well in agreement with previous studies (Sarotsakulchai et al. 2019). Based on previous times of minima along with TESS and ASAS data, we found that the orbital period of RW Dor is decreasing at a rate of -2.80×10^{-8} day yr^{-1} along with a cyclic variation. This suggests that material is transferring from the primary to the secondary component, driving the mass ratio of the system to increase. Assuming a conservative mass transfer rate from primary to secondary, it can be estimated from the following equation

$$\frac{\dot{P}}{P} = -3\dot{M}_1 \left[\frac{1}{M_1} - \frac{1}{M_2} \right]. \quad (2)$$

Assuming $M_1 = 0.52\ M_\odot$ and $M_2 = 0.82\ M_\odot$, $\dot{M}_1$ was found to be $4.64 \times 10^{-8}\ M_\odot\,\mathrm{yr}^{-1}$. The timescale of mass transfer is $M_1/\dot{M}_1 = 11.2$ Myr. The mechanism of angular momentum loss (AML) due to magnetic stellar wind has a tendency to decrease the orbital period during a timescale of 8.6 Myr (Sarotsakulchai et al. 2019). Based on the results of the present study, the time $P/\dot{P} = 10$ Myr, which is close to the value obtained from the AML mechanism. This indicates the magnetic stellar wind can also drive the decrease in the orbital period as the spot activity has been initiated in the source. These systems often go through thermal relaxation oscillation (TRO) along with the AML mechanism, whose period is of the order of a few million years (Qian 2001). As the period continues to decrease, the degree of contact between the components must increase. In the present study, we observed evidence of a cool spot on the primary component, suggesting that variable activity has been initiated which was not observed in earlier optical photometric or spectroscopic studies. This stellar activity would have triggered the AML and contributed to the decrease in the orbital period in RW Dor. In general, as the degree of contact increases it reduces the AML as the convective envelope probably veils the activity (e.g., Qian 2001). However, in the present scenario, it is not the case because of the appearance of the activity and this system has a shallow degree of contact ($f \sim 10\%$). Future observations are necessary in order to confirm the results as well as to track the stellar activity of the source.

6.2. Non-conservative Mass Loss in RW Dor

Justham et al. (2006) derived an analytical magnetic braking model assuming Ap/Bp stars for the formation of short period ($P < 1$ day) black hole low mass X-ray binaries and the AML

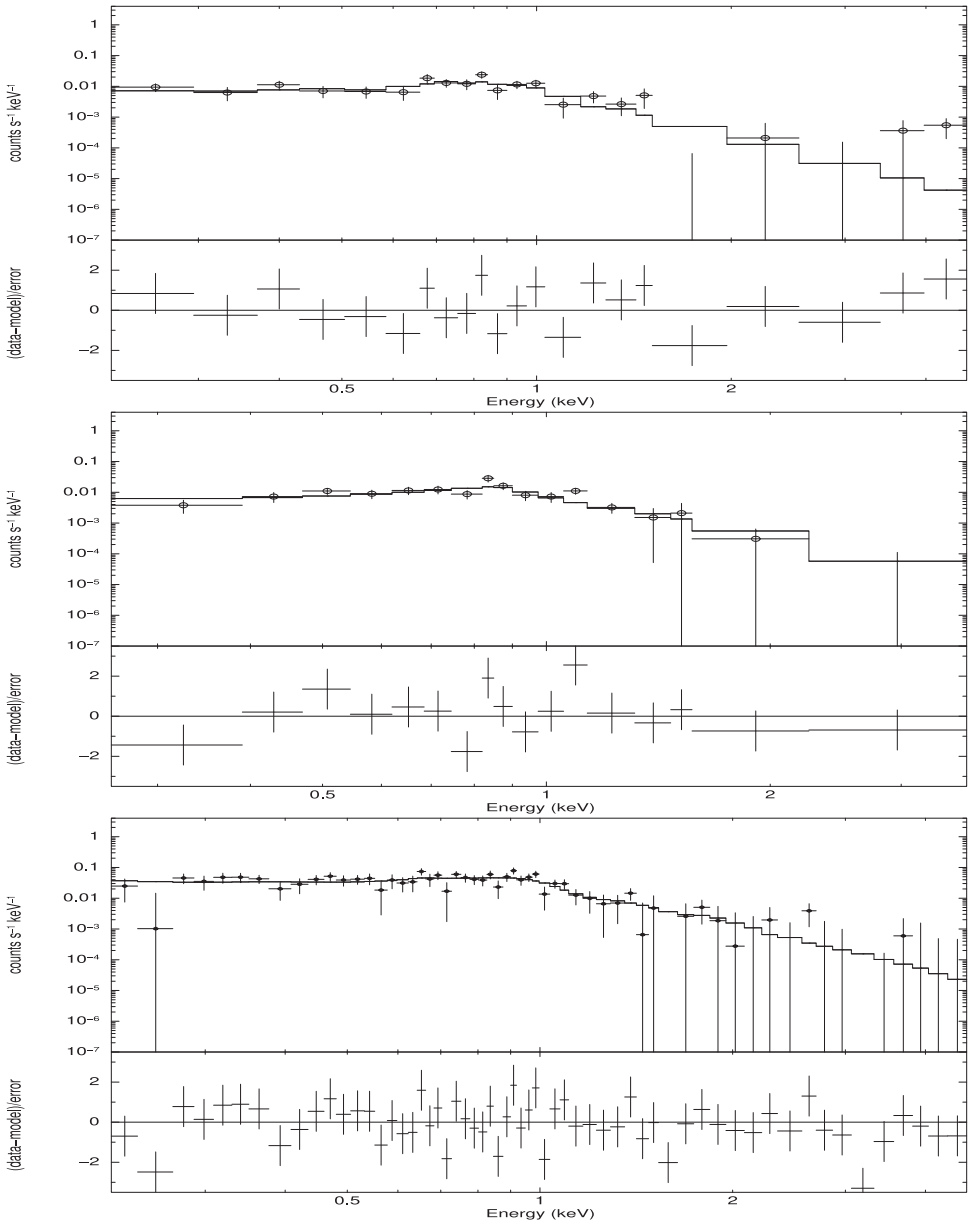

Figure 6. (a): The top panel shows the unfolded spectra along with the fit (thick line) for EPIC MOS1, MOS2 and PN. (b) The bottom panel displays the residuals. (c) The reference number is ObsID.0650020101 and observation date is 2010 December 11.

is given by

$$\dot{J}_{\rm amb} = -\frac{2\pi}{P}(GM)^{1/4} B_s R^{13/4} \dot{M}_{\rm wind}^{1/2}, \quad (3)$$

assuming $M_1 = 0.52\ M_\odot$, $R = 0.88\ R_\odot$, B_s (surface magnetic field) = 1000 G (upper limit) and $\dot{M}_{\rm wind} = 10^{-9}\ M_\odot\ {\rm yr}^{-1}$; $\dot{J}_{\rm amb}$ was estimated to be $-2.54 \times 10^{36}\ {\rm g\,cm^2\,s^{-2}}$ and for $\dot{M}_{\rm wind} = 10^{-10}\ M_\odot\ {\rm yr}^{-1}$ upper limit, $\dot{J}_{\rm amb} = -8.02 \times 10^{35}\ {\rm g\,cm^2\,s^{-2}}$. RW Dor's spectral properties are similar to another source, VW Cep, which has been extensively studied both in optical and X-ray bands (Mitnyan et al. 2018). The assumption of magnetic field $B = 1000$ G was based on observations of X-ray activity of VW Cep (Sanz-Forcada et al. 2007). Even a higher subsurface magnetic field of $B = 20$ kG is needed in VW Cep to explain the period modulation (Mitnyan et al. 2018). The angular momentum for a binary system can be written as

$$J_o = \frac{q}{(1+q)^2}(GM^3 a)^{1/2}, \quad (4)$$

where q is mass ratio 0.63, M is the total mass of the system and a is the semimajor axis in cgs units resulting in $J_o = 3.18 \times 10^{51}$ in cgs units. Based on the period variation,

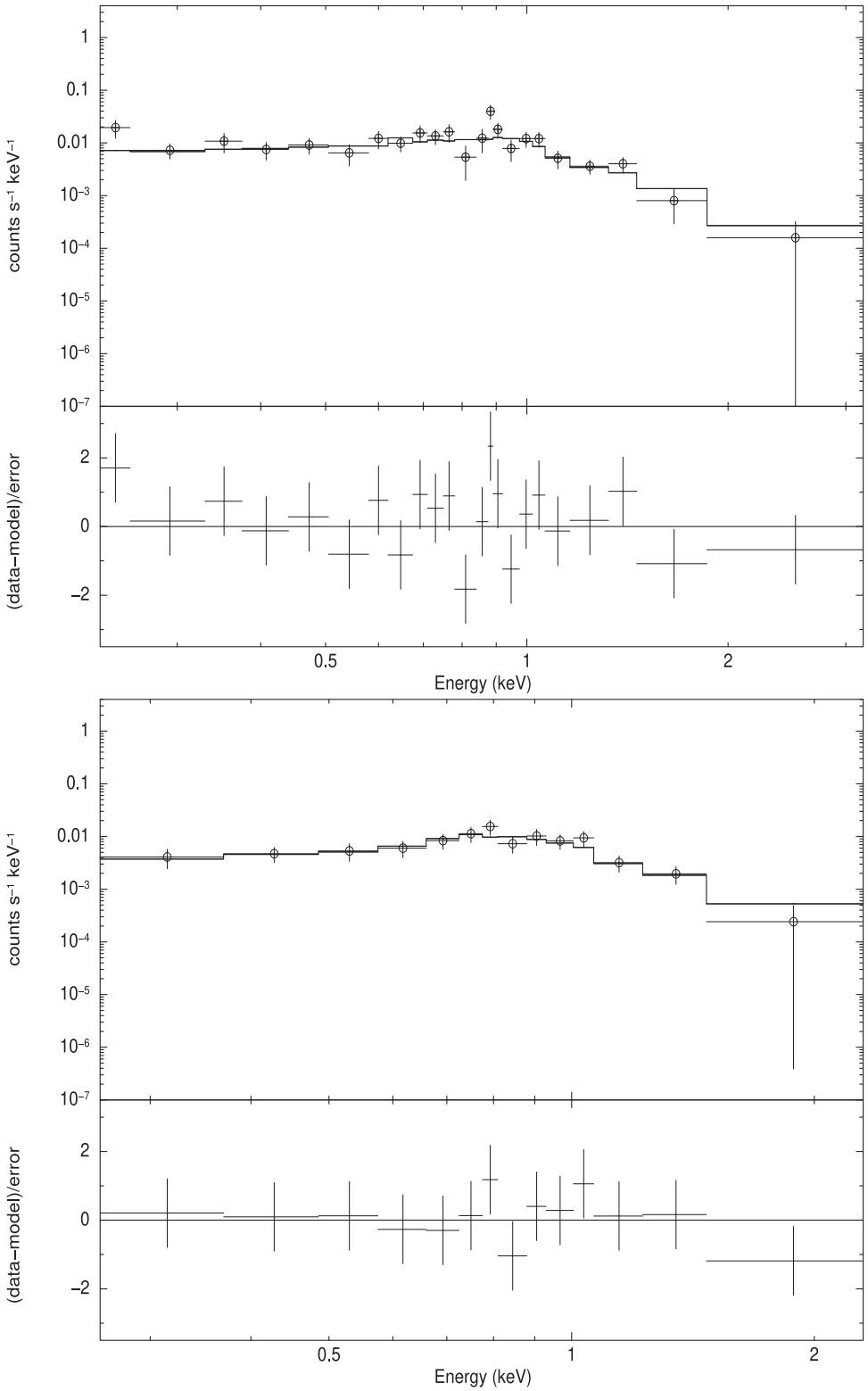

Figure 7. (a) The top panel shows the unfolded spectra along with the fit (thick line) for EPIC MOS1 and MOS2. (b): The bottom panel displays the residuals. The reference number is ObsID.0723650201 and observation date is 2013 October 22.

we estimated $\dot{P}/P = 9.81 \times 10^{-8}\,\mathrm{yr}^{-1}$ and the AML rate is found to be $\dot{J}_o = \frac{\dot{P}}{3P} J = 3.31 \times 10^{36}\,\mathrm{g\,cm^2\,s^{-2}}$. This value is a few times the value of $\dot{J}_{\mathrm{amb}}$. This indicates that the stellar wind also plays a key role in removing the angular momentum from the system and helps in decreasing the orbital period of the system. The location of the spot over the stellar surface also affects the AML in the system. In a simulation, it has been found that higher latitude spots can trigger relatively more AML when compared to a spot located at lower latitude (Cohen et al. 2009). Moreover, it was also noticed that there was a feedback mechanism, i.e., AML affects the stellar dynamo as it controls the stellar magnetic field distribution. In our present study, we noted the spot located at a colatitude of 32° which is closer to the pole of the star and hence would be extracting relatively more AML. For such a study in contact binaries, it is necessary to know the role of spot location and AML.

In the TRO model, as the material is transferring from primary to secondary, the decrease in the period should go along with an increase in the degree of contact, i.e., the CCE must be thick. However, we noted it is just 10% which is marginal contact in nature. There could be two possible reasons for such a configuration. The first one is Liu et al. (2019) proposed a mechanism where the period of the contact binaries varies and hence the evolution of q, from higher to lower values, is driven by the oscillatory nature of fill-out factor f which depends on the thickness of the CCE. It was shown that the increase or decrease of f can decrease the period of the system and would be able to trigger a merger of the system. In the present study, f was close to 10%, i.e., CCE is not thick, and the mass transfer from the CCE to either of the stellar components has been ongoing as there is not sufficient material in the CCE. Perhaps, as the f continues to decrease, the material in the CCE would be transferred to the accepter star, i.e., the secondary component which is the second phase in the model of Liu et al. (2018). Another phenomenon could be mass loss from the CCE which can drive away some of the angular momentum and decrease the orbital period.

It can be seen from $O-C$ that, initially, the period was increasing and later it was driven to a period decreasing trend. The increasing trend can be explained by assuming a conservative mass transfer from the secondary to the primary component, however, there could be a mass loss from one or both of the components. The mass loss can be estimated from the following equation (Tout & Hall 1991)

$$\dot{M}_1 = -\frac{M_1 + M_2}{2}\frac{\dot{P}}{P}, \tag{5}$$

assuming that the rate of mass transfer and loss is the same. We can equate $\dot{M}_1$ from Equation (2) and the above results in the quadratic equation in terms of q, i.e., $3q^2 + 2q - 3 = 0$, with one of the roots being $q \sim 0.72$. This indicates that at the high mass ratio, both mechanisms can drive the contact binary and this also can explain the low degree of contact as some mass is lost from the system.

Since RW Dor is displaying stellar activity in the form of the O'Connell effect, it is possible that the AML mechanism is occurring due to mass loss, which further helps in decreasing the orbital period. We assume that one of the components is driving the AML via mass loss, a situation which is described by Tout & Hall (1991)

$$\dot{M}_1 = \frac{M_1 M_2}{2(M_1 + M_2)}\left(\frac{d}{R_{\mathrm{A}}}\right)^2 \frac{\dot{P}}{P}. \tag{6}$$

Here R_{A} is the Alfvén radius and d is the distance between the binary components. An upper limit on Alfvén radius can be estimated by assuming $\beta = (d/R_{\mathrm{A}})^2$, and conservative mass transfer and mass loss due to AML is the same, then it can be shown that $q = M_2/M_1 = 3\beta - 2/3\beta + 2$ and for $q \sim 0.60$, $R_{\mathrm{A}} = d/1.63 = 7.9 \times 10^{10}$ cm which is similar to the size of the primary component radius.

A detailed study of the $O-C$ diagram was performed and light travel time effect (LITE) solutions with different epochs unveiled a third body with period $P_3 = 47.01 \pm 0.52$ yr (Figure 4, top panel), which is similar to the results reported by Sarotsakulchai et al. (2019) but with zero eccentricity. In our analysis, the eccentricity was found to be $e_3 = 0.21$ which was obtained after performing a systematic search of the best e_3 based on the least residuals. Since a few of the times of minima were old and may not be accurate, we estimated the possibility of a third body's orbital period by removing the times of minima before 1980 and noted a period of $P_3 = 27.22 \pm 3.12$ yr (see Figure 4, bottom panel). Such an orbital period of the third body was observed in VW Cep of about 31 yr (Kaszás et al. 1998), which has very similar properties except for the mass ratio. Another source, BH Cas, which exhibits similar properties to RW Dor and VW Cep also has a third body with $P_3 = 20.09$ yr (Liu et al. 2019). For RW Dor, the mass of the third body was noted to be $M_3 = 0.175\,M_\odot$ for $i = 90°$. We also looked for the third light in the TESS light curve but the data do not indicate any presence of it. Similar results were obtained in the previous study. Such a long period of third bodies is not rare and many of the contact binary systems have a third body with P_3 of more than 20 yr (Pribulla & Rucinski 2006; Rucinski & Pribulla 2007), and some of them have been optically confirmed. Future studies are needed to constrain the nature of third body solutions in RW Dor.

Generally, such a periodic modulation is ruled out based on the Applegate mechanism (Applegate 1992) because it requires quadruple momentum $\Delta Q \leqslant 10^{51}$–$10^{52}$ (Lanza & Rodonò 2002). Lanza & Rodono (1999) showed that magnetic energy is proportional to the quadruple moment perturbations. However, a more recent theory by Lanza (2020) where the orbital angular momentum is turned into spin angular momentum notes that the ΔQ is larger by a factor of

Table 4
Spectral Parameters Using a Bremsstrahlung Model and all the Error Bars at 90% Confidence Level

Parameter	Mos1(2009)	Mos1(2010)	Mos2(2010)	PN(2010)	Mos1(2013)	Mos2(2013)
kT (keV)	0.59 ± 0.12	0.59 ± 0.09	0.65 ± 0.14	0.50 ± 0.09	0.48 ± 0.09	0.45 ± 0.11
Norm ($\times 10^{-4}$)	2.97 ± 1.12	$3.51 \pm 1.06 \pm$	3.49 ± 0.92	2.21 ± 0.48	3.91 ± 1.15	3.27 ± 1.09
χ^2/(dof)	45/15	36/18	29/15	59/41	27/18	19/11

Table 5
Spectral Parameters for bbody

Parameter	Mos1(2009)	Mos1(2010)	Mos2(2010)	PN(2010)	Mos1(2013)	Mos2(2013)
kT (keV)	0.18 ± 0.01	0.16 ± 0.02	0.17 ± 0.01	0.18 ± 0.01	0.17 ± 0.01	0.17 ± 0.02
Norm_1 ($\times 10^{-6}$)	3.64 ± 0.49	3.42 ± 0.65	3.65 ± 0.56	2.80 ± 0.29	3.90 ± 0.65	3.22 ± 0.60
Flux (0.3–2.0 keV)	2.05	1.71	1.90	1.56	2.06	1.70
χ^2/(dof)	26/15	28/18	16/15	46/41	20/18	8/11

Note. Fluxes are in the unit 10^{-13} erg cm^{-2} s^{-1} and all the error bars are at the 90% confidence level.

Table 6
Spectral Parameters for Apec Model

Parameter	Mos1(2009)	Mos1(2010)	Mos2(2010)	PN(2010)	Mos1(2013)	Mos2(2013)
kT_1 (keV)	0.17 ± 0.07	0.30 ± 0.15	0.28 ± 0.11	0.24 ± 0.08	0.27 ± 0.14	0.29 ± 0.13
Z	0.44 ± 0.36	0.16 ± 0.11	0.09 ± 0.11	0.12 ± 0.08	0.11 ± 0.08	0.15 ± 0.07
Norm_1 ($\times 10^{-4}$)	0.83 ± 0.66	0.79 ± 0.57	2.81 ± 0.55	2.19 ± 1.13	3.20 ± 1.60	1.41 ± 1.30
kT_2 (keV)	0.87 ± 0.11	0.92 ± 0.23	0.82 ± 0.43	0.93 ± 0.15	1.03 ± 0.32	1.08 ± 0.44
Norm_2($\times 10^{-4}$)	0.96 ± 1.10	3.24 ± 1.65	2.34 ± 1.15	1.66 ± 0.65	1.84 ± 0.85	1.93 ± 0.81
Flux (0.3–2.0 keV)	1.83	1.80	1.65	1.61	2.15	1.83
L_X (10^{29} erg s^{-1})	3.33	3.28	3.00	2.93	3.92	3.33
EM_1($\times 10^{52}$ cm^{-3})	1.51	1.44	5.12	4.00	5.84	2.57
EM_1($\times 10^{52}$ cm^{-3})	1.75	5.91	4.27	3.03	3.35	3.52
χ^2/(dof)	13/12	23/15	16/11	16/55	19/15	5/8

Note. Fluxes are in the unit 10^{-13} erg cm^{-2} s^{-1} and all the error bars are at the 90% confidence level.

100–1000. Sarotsakulchai et al. (2019) explained the periodic variations using the presence of a third body and ruled out the magnetic activity. With the new theory put forward by Lanza (2020), now the magnetic activity cycle can be one of the viable mechanisms for the observed periodic modulation as observed in this source.

6.3. Loop Size Emitting the Quiescent X-Ray Emission in RW Dor

For a few contact binaries coronal emission temperatures are known. In Table 4, we show the X-ray spectral parameters of four contact binaries including RW Dor from the present work. Three contact binaries, viz. RW Dor, VW Cep and 44 Boo, have similar orbital periods and spectral types. Among these four systems, BH Cas has the highest X-ray luminosity, i.e., $L_X = 92.5 \times 10^{29}$ erg s^{-1} and others have similar L_X (Table 4).

Based on present studies, it can be concluded that during the X-ray observations by XMM-Newton, RW Dor and other contact binaries (VW Cep; Gondoin 2004a, 44 Boo; Gondoin 2004b, and BH Cas; Liu et al. 2019) were in a quiescent state for some duration. The exact reason for coronal X-ray emission in a quiescent state is debatable in terms of the distribution of magnetic field structures but the presence of loops cannot be ruled out. Ventura et al. (1998) explained the quiescent emission using two distinct classes of loops associated with the corona in G-type stars. One of the coronal loops is cooler with a temperature $T_{\max} \sim 1.5$–5×10^6 K and the other one is relatively hotter with a temperature 1–3 $\times$ 10^7 K. A detailed loop modeling is not possible for the present work but the observed temperature (see Table 7) from the X-ray spectra does indicate the presence of such loops primarily based on the coronal temperatures, viz. 0.27 and 1.03 keV (year 2013) (3.1 and 12 MK).

Table 7
Comparison of X-Ray Spectral Parameters of Four Contact Binaries along with Other Parameters

Parameter	RW Dor	VW Cep	BH Cas	44 Boo
	Present work	Mitnyan et al. (2018), Gondoin (2004a)	Liu et al. (2019)	Gondoin (2004b)
kT_1 (keV)	0.28	0.26	0.13/ 0.26[a]	0.25
kT_2 (keV)	0.82	0.56	⋯	0.65
L_X 10^{29} erg s^{-1}	3.3	6.28	92.5	2.24
P (days)	0.285	0.278	0.405	0.267
q (mass ratio)	0.61	0.30	0.47	0.49
$\dot{P}$ (day yr^{-1})	2.8 ↓	18.5 ↓	32.7 ↑	⋯

Notes. Up and down arrow symbols signify increase and decrease in period respectively.
[a] Estimated from blackbody and bremsstrahlung models.

Assuming that the loop systems are not dynamic and each loop consists of similar nonvarying pressure p, temperature T (K) and cross-section, then a loop length scale (L) can be obtained (Mewe et al. 1982) using the relation $T = 1400(pL)^{1/3}$ (Rosner et al. 1978)

$$L_{10} = 7.4 \times F \times T_7^4 \times \mathrm{EM}_{52}^{-1} \times (R/R_\odot)^2, \quad (7)$$

where L_{10} is the loop half length in units of 10^{10} cm, T_7 is the coronal region temperature in units of 10^7 K, EM_{52} is the emission measure in units of 10^{52} cm^{-3} and F is the filling factor. Actually, F is a difficult parameter to calculate as it depends on many parameters of the loop, for example, the area of the loop. In the case of RW Dor, it is not known, however for 44 Boo, F was reported to be 50%–70% (Gondoin 2004b). Adopting a value of $F = 0.7$, $R = 0.88$ $R_\odot$ and the rest of the values of parameters from Table 7, we estimated $L = 1 \times 10^{10}$ cm for temperature 0.93 keV (PN 2010). For other coronal temperatures, it varies from 0.1 to 6×10^9 cm. These values can be considered as upper limits due to uncertainty in the value of F. It can be observed that the estimated loop size from X-ray spectra is almost 7–8 times lower than that estimated from the Alfvén radius. There are many approximations in estimating the loop length as discussed with one of them being the constant loop cross-section. If one considers a non-uniform cross-section of the order of 10 (Schrijver 1987; with 1 being a uniform cross-section) then the loop size increases. The estimated loop sizes are close to the sizes seen in 44 Boo and VW Cep (O'Connell 1951; Gondoin 2004b). Perhaps the estimated smaller loop size could be due to the fact that during the X-ray observations, the source was in a quiescent state, hence the estimated loop size was smaller. Now during the TESS observations, it is probably higher due to enhanced activity.

7. Conclusions

Optical and X-ray studies have been carried out for a marginal contact binary RW Dor using TESS and XMM-Newton telescopes. For the first time, we report the variable O'Connell effect in the light curve and the maximum asymmetry in the light curve can be explained by a stellar spot of size 15° on the primary component at HJD 2458489.2509. Using new times of minima, we produce a robust estimate of the third body orbital period $P_3 \sim 47$ yr with an eccentricity $e_3 = 0.21$. We show that non-conservative mass loss plays a key role in the evolution of the binary apart from conservative mass transfer from the primary to the secondary component. The X-ray luminosity did not vary significantly during three different occasions of observation, indicating a constant X-ray quiescent emission from the source. Assuming that the quiescent emission arises from an undisturbed loop, its size was estimated to be around $0.6–1.0 \times 10^{10}$ cm. Future observations in optical and X-ray energy bands would be helpful to understand the nature of coronal geometry in RW Dor and the associated activity.

Acknowledgments

We acknowledge the referee for the comments which improved the quality of the work. K.S. acknowledges the financial support from the SERB Core Research Grant project, the Government of India. Mamatha Rani acknowledges the support from the SRF INSPIRE (IF 170314) fellowship program, Government of India. This paper includes data collected by the TESS mission where funding is provided by the NASA Explorer Program. Gaia data are being processed by the Gaia Data Processing and Analysis Consortium (DPAC). Funding for the DPAC is provided by national institutions, in particular, the institutions participating in the Gaia MultiLateral Agreement (MLA). The Gaia mission website is https://www.cosmos.esa.int/gaia. The Gaia archive website is https://archives.esac.esa.int/gaia. This work also uses data obtained by XMM-Newton, an ESA science mission with instruments and contributions directly funded by ESA Member States and the USA (NASA).

Data Availability

Data used in this work can be accessed through the HEASARC website (https://heasarc.gsfc.nasa.gov/cgi-bin/W3Browse/w3browse.pl) and are also available with the authors.

References

Applegate, J. H. 1992, ApJ, 385, 621
Arnaud, K. A. 1996, in ASP Conf. Ser. 101, Astronomical Data Analysis Software and Systems V, ed. G. Jacoby & J. Barnes (San Francisco, CA: ASP), 17
Binnendijk, L. 1970, VA, 12, 217

Buzasi, D. L. 1997, ApJ, 484, 855
Carroll, R. W., Cruddace, R. G., Friedman, H., et al. 1980, ApJL, 235, L77
Chen, W. P., Sanchawala, K., & Chiu, M. C. 2006, AJ, 131, 990
Cohen, O., Drake, J. J., Kashyap, V. L., & Gombosi, T. I. 2009, ApJ, 699, 1501
Deb, S., & Singh, H. P. 2011, MNRAS, 412, 1787
Dickey, J. M., & Lockman, F. J. 1990, ARA&A, 28, 215
Duerbeck, H. W., & Rucinski, S. M. 2007, AJ, 133, 169
Gondoin, P. 2004a, A&A, 415, 1113
Gondoin, P. 2004b, A&A, 426, 1035
Hendry, P. D., & Mochnacki, S. W. 2000, ApJ, 531, 467
Hilditch, R. W., Hill, G., & Bell, S. A. 1992, MNRAS, 255, 285
Hu, et al. 2016, AJ, 833, 9
Huenemoerder, D. P., Testa, P., & Buzasi, D. L. 2006, ApJ, 650, 1119
Jardine, M., & Unruh, Y. C. 1999, A&A, 346, 883
Justham, S., Rappaport, S., & Podsiadlowski, P. 2006, MNRAS, 366, 1415
Kaluzny, J., & Caillault, J.-P. 1989, AcA, 39, 27
Kaszás, G., Vinkó, J., Szatmáry, K., et al. 1998, A&A, 331, 231
Kopal, Z. 1959, Close Binary Systems (London: Chapman and Hall)
Lanza,, Rodonò, et al. 1999, A&A, 349, 887
Lanza, A. F. 2020, MNRAS, 491, 1820
Lanza, A. F., & Rodonò, M. 2002, AN, 323, 424
Liu, L., Qian, S. B., & Xiong, X. 2018, MNRAS, 474, 5199
Liu, J, et al. 2019, PASJ, 131, 1
Lucy, L. B. 1967, ZA, 65, 89
Lucy, L. B. 1968, ApJ, 151, 1123
Marino, B. F., Walker, W. S. G., Bembrick, C., & Budding, E. 2007, PASA, 24, 199
Marton, S. F., Grieco, A., & Sistero, R. F. 1989, MNRAS, 240, 931
McGale, P. A., Pye, J. P., & Hodgkin, S. T. 1996, MNRAS, 280, 627
Mewe, R., Gronenschild, E. H. B. M., Heise, J., et al. 1982, ApJ, 260, 233
Mitnyan, T., et al. 2018, A&A, 612, A91
O'Connell, D. J. K. 1951, PRCO, 2, 85
Pribulla, T., & Rucinski, S. M. 2006, AJ, 131, 2986
Prsa, A., & Zwitter, T. 2005, ApJ, 628, 426
Qian, S. 2001, MNRAS, 328, 635
Qian, S. B., et al. 2017, RAA, 17, 087
Ricker, G. R., Winn, J. N., Vanderspek, R., et al. 2015, Proc. SPIE, 1, 014003
Rosner, R., Tucker, W. H., & Vaiana, G. S. 1978, ApJ, 220, 643
Ruciński, S. M. 1969, AcA, 19, 245
Rucinski, S. M., & Pribulla, T. 2007, AJ, 134, 2353
Sanz-Forcada, J., Favata, F., & Micela, G. 2007, A&A, 466, 309
Sarotsakulchai, T., et al. 2019, PASJ, 71, 34
Schrijver, C. J. 1987, A&A, 180, 241
Smith, R. K., Brickhouse, N. S., Liedahl, D. A., & Raymond, J. C. 2001, ApJL, 556, L91
Sriram, K., Malu, S., Choi, C. S., & Vivekananda Rao, P. 2016, AJ, 151, 69
Sriram, K., Malu, S., Choi, C. S., & Vivekananda Rao, P. 2017, AJ, 153, 231
Sriram, K., Malu, S., Choi, C. S., & Vivekananda Rao, P. 2018, AJ, 155, 172
Stępien, K., Schmitt, J. H. M. M., & Voges, W. 2001, A&A, 370, 157
Tout, C. A., & Hall, D. S. 1991, MNRAS, 253, 9
Tran, K., Levine, A., Rappaport, S., et al. 2013, ApJ, 774, 81
van Hamme, W. 1993, AJ, 106, 2096
Ventura, R., Maggio, A., & Peres, G. 1998, A&A, 334, 188
Vilhu, O., & Maceroni, C. 2007, in IAU Symp. 240, Binary Stars as Critical Tools & Tests in Contemporary Astrophysics, ed. W. I. Hartkopf, E. F. Guinan, & P. Harmanec (Cambridge: Cambridge Univ. Press), 462
Zasche, P., Liakos, A., Niarchos, P., et al. 2009, NewA, 14, 121